Environmental Science & Technology

Article

pubs.acs.org/est

Sequestration of Selenium on Calcite Surfaces Revealed by Nanoscale Imaging

Christine V. Putnis,[†] François Renard,*[,‡,§] Helen E. King,[†] German Montes-Hernandez,[⊥] and Encarnacion Ruiz-Agudo[∥]

[†]Institut für Mineralogie, University of Münster, Corrensstrasse 24, 48149 Münster, Germany

[‡]ISTerre, Univ. Grenoble Alpes, BP 53, F-38041 Grenoble, France

[§]Physics of Geological Processes, University of Oslo, Oslo, Norway

[∥]Department of Mineralogy and Petrology, University of Granada, Fuentenueva s/n 18071, Granada, Spain

[⊥]CNRS, ISTerre, BP 53, F-38041 Grenoble, France

Supporting Information

ABSTRACT: Calcite, a widespread natural mineral at the Earth's surface, is well-known for its capacity to sequester various elements within its structure. Among these elements, selenium is important because of its high toxicity in natural systems and for human health. In the form of selenite ($Se^{(IV)}$), selenium can be incorporated into calcite during growth. Our in situ atomic force microscopy observations of calcite surfaces during contact with selenium-bearing solutions demonstrate that another process of selenium trapping can occur under conditions in which calcite dissolves. Upon the injection of solutions containing selenium in two states of oxidation (either $Se^{(IV)}$ or $Se^{(VI)}$), precipitates were observed forming while calcite was still dissolving. In the presence of selenate ($Se^{(VI)}$), the precipitates formed remained small during the observation period. When injecting selenite ($Se^{(IV)}$), the precipitates grew significantly and were identified as $CaSeO_3 \cdot H_2O$, based on SEM observations, Raman spectroscopy, and thermodynamic calculations. An interpretation is proposed where the dissolution of calcite increases the calcium concentration in a thin boundary layer in contact with the surface, allowing the precipitation of a selenium phase. This process of dissolution−precipitation provides a new mechanism for selenium sequestration and extends the range of thermodynamic conditions under which such a process is efficient.

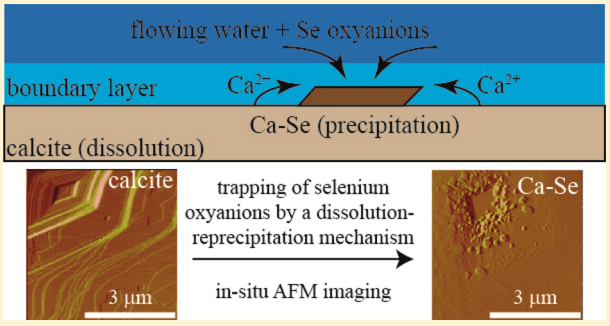

INTRODUCTION

Calcium carbonate, a major constituent of the rocks in the Earth's upper crust, has the ability to trap several kinds of ions in its structure. Among them, cations[1−4] and anions[5−7] could be incorporated or interact with mineral surfaces, making calcite a potential sink for these elements on the global scale. Several studies have characterized how arsenic, phosphate, or selenite oxyanions could be incorporated during the growth of calcite crystals, either under surface conditions[8,7] or under hydrothermal conditions.[9] In these studies, the incorporation of the ions into calcite during calcite precipitation was the main mechanism of sequestration as they could replace either the calcium atoms or the carbonate groups in the crystalline system of calcite, controlling both the kinetics of reaction and the growth and dissolution mechanisms.[10,11]

Selenium is an important oxyanion on the global scale,[12] and its interaction with calcite has several environmental applications such as the remediation of radioactive selenium ^{79}Se, the concentration of selenium in agricultural soils due to irrigation, the contamination of soils by acid mine drainage, and the effect of selenium on human health due to its concentration in drinking waters or its bioaccumulation in food. In fact, selenium is the element with the smallest difference between dietary (<40 μg/day) and toxic (>400 μg/day) effects on humans,[13] such that international agencies have defined a strict reference value for selenium consumption, close to 55 μg/day.[14]

Selenium can exist in nature in several states of oxidation: $Se^{(-II)}$ in anoxic reductive environments and/or contained in organic molecules, elemental selenium $Se^{(0)}$, and two main oxidized forms $Se^{(IV)}$ and $Se^{(VI)}$. These last two forms exist as oxyanions $Se^{(IV)}O_3^{2-}$ and $Se^{(VI)}O_4^{2-}$ that could interact with calcite via adsorption or incorporation processes. Selenium speciation analyses in various fresh water environments indicate the domination of either the $Se^{(IV)}$ species in rain waters or the $Se^{(VI)}$ species in rivers, groundwater, and snow. It is noticeable

Received: August 22, 2013
Revised: November 8, 2013
Accepted: November 13, 2013
Published: November 13, 2013

that in sea and oceanic waters, $Se^{(IV)}$ concentration is usually several times smaller than $Se^{(VI)}$.[15]

Selenium oxyanions may be incorporated into calcite during its growth either under surface conditions[16] or under hydrothermal conditions.[9] This element has also been shown to be remobilized when carbon dioxide is injected,[17] for example during the leakage of an underground carbon dioxide repository.[18] However, no study has been performed to characterize how selenium interacts with calcite during its dissolution. In the present study, we analyze such a situation, by imaging on the nanometer scale the interaction between selenium oxyanions ($Se^{(IV)}$ and $Se^{(VI)}$) and calcite surfaces under far-from-equilibrium conditions where calcite dissolves. For this, we used a flow-through cell coupled to an atomic force microscope. Our experiments are performed under conditions where we demonstrate the existence of a dissolution–reprecipitation process within a boundary layer at the mineral–water interface, allowing the simultaneous dissolution of calcite and precipitation of a selenium phase. This coupled process may control the localization of selenium in natural environments. It also provides a new mechanism for selenium trapping on calcite. More generally, our direct observations show that fluid-rock reactions can be controlled by mechanisms occurring in a fluid boundary layer at the mineral surface, confirming the crucial role of the mineral–water interface where the reactions between minerals and their environment take place.[19]

METHODOLOGY

Solutions and Calcite. A calcite crystal (Iceland spar, Vizcaya, Mexico) was obtained from the Natural History Museum in London. ICP-OES (inductively coupled plasma–optical emission spectroscopy) revealed the high purity of the crystal, with only trace amounts of Mn (31 ppb), Mg (2.8 ppb), and Sr (11.4 ppb) detected. Rhombohedral fragments (ca. 4 × 2 × 1 mm) were cleaved directly before each experiment from this single calcite crystal, parallel to the (10−14) cleavage plane. Two kinds of aqueous solutions were used in the dissolution experiments. First, selenium-free freshwater solutions with controlled pH, between 7 and 9, and ionic strength equal either to zero or to 2.6×10^{-3} M were injected in a flow-through fluid cell to dissolve the calcite surface. These solutions were prepared using doubled deionized water (resistivity >18 mΩ cm^{-1}) directly before each experiment. Sodium chloride and sodium hydroxide were used to adjust ionic strength and pH, respectively. Then, solutions with selenium(IV) or (VI) oxyanions at a 70 or 200 ppm concentration, with the same pH and ionic strength as the aqueous solutions initially used, were injected in the fluid cell (see Table 1). The selenium solutions were prepared from salts of sodium selenate (Merk) and pentahydrate sodium selenite (Fluka) dissolved into double deionized water. The pH and salinity were adjusted according to thermodynamic simulations using the PHREEQC software.[20] As well, the pH of several solutions was measured independently using a pH meter, confirming the PHREEQC simulation results.

Atomic Force Microscopy. The calcite surfaces were scanned using a Bruker Multimode Atomic Force Microscope (AFM) operating in contact mode. The experiments were performed in situ within an O-ring sealed flow-through fluid cell from Digital Instruments. At regular time intervals between each scan (lasting 1.5 min), the fluids were injected with a syringe, giving an effective flow rate of 22 μL s^{-1}. Prior test experiments using gravity feed continuous flow with constant solution height were made to confirm the observations. Furthermore, this flow rate ensures that there is no significant influence of the diffusion to the bulk on the dissolution process, as inferred from the fact that the measured dissolution rate is not affected when increasing the flow rate above this value (see for example Ruiz-Agudo et al.[24]). AFM images were collected

Table 1. List of AFM Experiments, Composition of the Two Fluids Injected, and Observations of Precipitates[a]

exp. no.	water solution	selenium solution	observations	fluid sampl.	SEM/ Raman
Se13	pH = 7	200 ppm $Se^{(IV)}$	formation of many precipitates that cover the surface		
	IS = 0	pH = 9.1			
		IS = 7.6×10^{-3}			
Se14	pH = 7	200 ppm $Se^{(VI)}$	formation of small precipitates		yes
	IS = 0	pH = 7			
		IS = 7.6×10^{-3}			
Se15	pH = 7	200 ppm $Se^{(IV)}$	many precipitates that grow in etch pits and near steps		yes
	IS = 0	pH = 9.1			
		IS = 7.6×10^{-3}			
Se16	pH = 7.3 (meas.)	70 ppm $Se^{(VI)}$	randomly located tiny precipitates (<100 nm)		
	IS = 2.6×10^{-3}	pH = 6.5 (meas.)			
		IS = 2.6×10^{-3}			
Se17	pH = 8.5 (meas.)	70 ppm $Se^{(IV)}$	many precipitates nucleate on the obtuse angle of the etch pits; large precipitates form after 1 h and cover the whole surface		yes
	IS = 2.6×10^{-3}	pH = 8.5 (meas.)			
		IS = 2.6×10^{-3}			
Se18	pH = 8.5 (meas.)	70 ppm $Se^{(IV)}$	same as Se17		yes
	IS = 2.6×10^{-3}	pH = 8.5 (meas.)			
		IS = 2.6×10^{-3}			
Se19	pH = 7.3 (meas.)	70 ppm $Se^{(VI)}$	few tiny precipitates (~100 nm diameter)	yes	yes
	IS = 2.6×10^{-3}	pH = 7.3 (meas.)			
		IS = 2.6×10^{-3}			
Se20	pH = 8.5 (calc.)	70 ppm $Se^{(VI)}$	few tiny precipitates		
	IS = 2.6×10^{-3}	pH = 8.5 (calc.)			
		IS = 2.6×10^{-3}			
Se21	pH = 7 (calc.)	70 ppm $Se^{(IV)}$	same as Se17	yes	
	IS = 2.6×10^{-3}	pH = 7 (calc.)			
		IS = 2.0×10^{-3}			
Se22	pH = 8.5 (meas.)	70 ppm $Se^{(IV)}$	same as Se17	yes	
	IS = 2.6×10^{-3}	pH = 8.5 (meas.)			
		IS = 2.6×10^{-3}			

[a]Samples where the fluid composition was analyzed are indicated, as well as those for which SEM and Raman studies were performed.

using Si_3N_4 tips (Veeco Instruments, tip model NP-S20) with spring constants of 0.12 N m^{-1} and 0.58 N m^{-1}. Images were analyzed using the NanoScope software (version 5.31r1). Measurements of step retreat velocity (or etch pit spreading rate) were made from sequential images scanned in the same direction. The retreat velocity v_{sum} (nm s^{-1}) given by $v_{sum} = (v_+ + v_-)$ (where v_+ and v_- are the retreat velocities of + and − steps, respectively) was calculated measuring the length increase per unit time between opposite parallel steps in sequential images.

For representative experiments (see Table 1), the outlet fluid was sampled, collecting a sequence of four aliquots of 10 mL (the outflow from five consecutive scans) that were later analyzed for calcium and selenium concentration using ICP-OES.

Raman Spectroscopy. A Raman spectrometer (Horiba XploRA) operating with the 532 nm line of a Nd:YAG laser was used for the analysis of surface precipitates on calcite after contact with selenium-bearing solutions. Reference spectra for the calcite sample, the sodium selenate, and the pentahydrate sodium selenite were taken with a 500 μm hole, 100 μm slit, and 1800 grooves per millimeter grating (see Supporting Information). Each spectrum was taken for 2 s, 30 times, and the results were averaged to increase the signal-to-noise ratio. Then three samples (Se14, Se17, and Se18) that had undergone interaction with selenium were selected for Raman investigations. Spectra were taken with a 100 μm hole, for 30 s, 20 times. For each of these three samples, a flat area and etch pit areas were measured to search for Raman bands characteristic of selenate or selenite vibrations. The spectra were corrected for system drift using the 520.7 nm Raman band of silicon taken at the beginning and the end of the Raman measuring session. The Fityk program[21] was used to remove the background using a linear function followed by fitting the Raman bands using a Voigt function.

Scanning Electron Microscopy Observations. Five samples used in AFM experiments (Se14, Se15, Se17, Se18, Se19) were left in 5 mL of the corresponding selenium-bearing solution for 12 h to ensure that equilibrium between the solid phases and the fluid had been reached and then immediately dried by absorbing the fluid with filter paper. They were then left for 30 min in an oven at 50 °C to remove adsorbed water and coated with a 20-nm-thick layer of carbon. Observations were made with a JEOL JSM-6610LV scanning electron microscope (SEM) operating at 15 kV. EDX (energy dispersive X-ray analysis) was performed in the SEM using Oxford Instruments Inca software.

Geochemical Modeling Using PHREEQC Software. Solution composition and ion adsorption (by surface exchange reactions) upon contact of calcite with the selenium-bearing solutions used in the AFM experiments was simulated using the hydro-geochemical software PHREEQC, version 2.18.3.5570. The minteq dat database was supplemented with data for the hydrolysis and soluble complexes of Se species available in the literature (Tables S1 and S2). Thermodynamic data of the most likely calcium selenate and selenite phases were also taken from the literature.[22] Surface exchange of selenite with carbonate on calcite was simulated using exchange constants and surface site density (1.02×10^{-5} sites m^{-2}) from Cowan et al.[23]

RESULTS AND DISCUSSION

Effect of Selenium on Calcite Dissolution. Direct in situ observations show that when in contact with water at the same pH and ionic strength of selenium bearing solutions, the (10−14) calcite surface starts dissolving along steps that retreat and through the formation of etch pits with typical rhombohedral shapes (Figure 1a; e.g., refs 24 and 11). Measured retreat rates

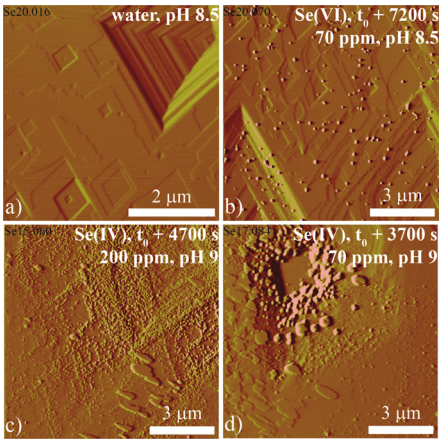

Figure 1. In-situ Atomic Force Microscopy (AFM) images of calcite surfaces during dissolution in a flow-through cell. (a) Dissolution with selenium free water, showing typical rhombohedral etch pits. (b) Dissolution in the presence of selenate ($Se^{(VI)}$), 70 ppm, same pH as in a, showing the formation of tiny precipitates. (c, d) Dissolution in the presence of selenite ($Se^{(IV)}$), at 200 or 70 ppm concentration, showing massive precipitation on the calcite surface. Precipitates mainly localize along steps or in etch pits where dissolution is faster. t_0 corresponds to the time of selenium injection.

(v_{sum}) in water ranged between 1.3 and 3.3 nm s^{-1}. These values agree well with previously published values of etch pit spreading or retreat rates for calcite in dilute solutions at circumneutral pH (see, for example, the review by Ruiz-Agudo and Putnis[11] and references therein). Measured values in selenium-bearing solutions ranged from 2.1 up to 4.2 nm s^{-1}. In general, the presence of both $Se^{(IV)}$ and $Se^{(VI)}$ tended to increase the etch pit spreading rate, although in the presence of $Se^{(IV)}$, faster etch pit spreading rates were measured. As well, increasing the concentration of selenium from 70 up to 200 ppm resulted in higher values of etch pit spreading rate. No significant effect was observed upon increasing the pH up to 9.

Note that the fluid injected has the same pH and ionic strength as the initial selenium-free solution, so any effect observed in the kinetics of calcite dissolution is exclusively due to the presence of selenium in the solution. It has been shown that SeO_3^{2-} ions adsorbs chemically onto (10−14) calcite surfaces with their oxygen triangular base lying on the (0006) plane via surface ion exchange of up to 2% of the carbonate groups at the surface,[23,25] while just trace amounts of selenate are adsorbed onto the carbonate site of calcite. One possible explanation for our observations is that the adsorption of these Se species enhances dissolution by lowering the activation energy for detachment of Ca at the step edge. The evidence for this is as follows: (1) Sorption of an anion has been shown to aid attachment/detachment of cations from planar mineral surfaces.[26] (2) Cation detachment from steps has been shown to be rate-limiting.[27] (3) The composition of the solution (e.g., the presence of foreign ions or electrolytes) can change step velocities.[24,28,29] This evidence tends to indicate that specific adsorption of Se at step edges (and preferentially selenite due to its shape matching) aids the rate-limiting detachment of Ca and hence increases the dissolution rate. This mechanism also

explains the immediate formation of Ca−Se precipitates near the step edges during dissolution because if there are preadsorbed Ca−Se complexes forming as the steps retreat, the saturation needed for heterogeneous nucleation would be lower. Furthermore, the higher rates measured in the presence of $Se^{(IV)}$ compared to $Se^{(VI)}$ could present indirect evidence of either enhanced Ca release through preferential anion adsorption or a more distorted surface structure in the former case and could be explained by considering the higher amounts of $Se^{(IV)}$ adsorbed on calcite surfaces. Another possible and likely explanation would be that the calcite rate of dissolution is promoted in the presence of selenium by a simple physicochemical effect, i.e., the consumption of liberated Ca^{2+} forming Se−Ca-bearing complexes and clusters. This allows the fluid to be more depleted with respect to calcium and maintained far-from-equilibrium conditions compared to Se-free solutions and hence promote further dissolution, as evidenced by increased etch pit spreading rates in the presence of selenium-bearing solutions.

AFM Imaging of the Growth of Ca−Selenite and Ca−Selenate Phases onto Calcite Cleavage Surfaces. Together with a faster dissolution, as soon as selenium-bearing solutions with a fixed concentration of selenium oxyanions (70 or 200 ppm) were introduced into the fluid cell, precipitates were immediately observed forming on the calcite surfaces. In our experiments, nucleation and precipitation occurred predominantly at multiple step edges such as the deep etch pits seen in Figure 2. Small, scarce particles, less than 100 nm wide and possibly smaller and several nanometers thick, precipitate when a selenate ($Se^{(VI)}$) solution is injected (Figure 1b) and remain as such (i.e., no further growth was detected in the AFM images) after 1 h of continuous flow of the selenate-bearing solution. Conversely, when selenite ($Se^{(IV)}$) solutions are injected into the fluid cell, large amounts of precipitates form, covering the whole scanned surface in less than 1 h of continuous solution flow. These precipitates initiate as small particles that slowly grow into platy forms up to 500 nm long (Figure 1c), limited by well-defined straight edges. This is an indication of its possible crystalline nature. They nucleate predominantly along dissolving step edges or inside deeper etch pits where multiple step edges exist on the calcite surface (Figure 1d). Figure 2 shows a time sequence of a 5 × 5 μm surface area upon injection of the selenite-bearing solution. It was found that nucleation starts immediately after the injection and the precipitates form while calcite is still dissolving (note that etch pits are still expanding while the new phase was nucleating). The adhesion of this new phase to the calcite surface was initially weak, as revealed by the fact that some particles were moved by the tip of the AFM during scanning. After several minutes, adhesion to the substrate underneath is strong enough to avoid this effect. After a couple of minutes, the precipitates reach a thickness of several nanometers (see below) and, occasionally, thicknesses of up to 350 nm were measured upon long reaction times (Figure 3a).

Identification of the Precipitate. AFM gives topographical analysis of a surface and direct observations during experiments. However, so far during in situ AFM experiments in a fluid cell, simultaneous chemical analysis of the surface is not possible. Therefore, chemical analysis and phase identification had to be performed ex situ. In order to verify the composition of the precipitates formed during dissolution of calcite in the presence of selenium-bearing solutions, SEM and Raman spectroscopy analyses were performed once the crystals

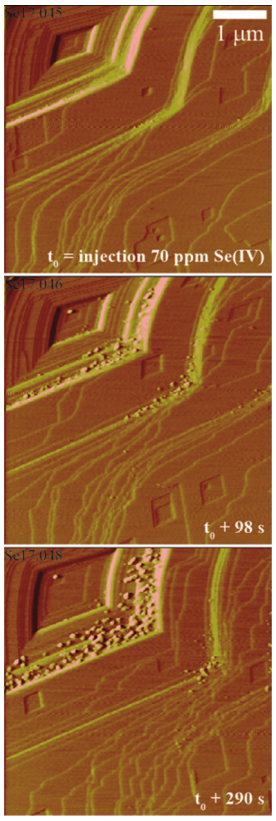

Figure 2. Time-lapse in situ AFM images of calcite surfaces during dissolution−precipitation in a flow-through cell. Top: the calcite surface displays a typical dissolution pattern, with retreating steps and a large etch pit on the top left of the picture. t_0 corresponds to the injection time of a solution containing 70 ppm selenite. Middle: After 98s, some precipitates have formed, mainly along steps and in the etch pit. Bottom: Same surface after 290 s. In these images, the etch pit grows, indicating calcite dissolution, and at the same time, precipitation of a selenium phase occurred, demonstrating a coupled dissolution−precipitation process.

were taken from the AFM fluid cell and dried. Unfortunately, in the case of selenate, the particles were too small to identify their composition by EDX or Raman spectroscopy. In fact, Raman analysis shows no band other than those belonging to the calcite substrate on the surface that was reacted in the presence of $Se^{(VI)}$. However, for selenite some large precipitates (Figure 3a) could be analyzed by these means. Raman spectra of these particles showed two bands at 752 and 832 cm^{-1} not observed in the case of pure calcite (Figure 4). These peaks are slightly shifted to higher wavenumbers than the bands in sodium selenite (Figure S1), consistent with the difference observed in carbonate compounds between sodium and calcium bearing phases (see Supporting Information). Thus, the precipitated phase is interpreted to be a calcium-bearing selenite phase. The presence of broad bands in comparison to the sharper bands present in the sodium selenite reference spectrum indicates that the precipitated phase was not highly crystalline. Additionally, EDX analysis clearly shows the presence of selenium and calcium in the precipitate, confirming the information obtained by Raman spectroscopy. Furthermore, ICP-OES analyses of the solutions collected after exiting the AFM flow-through cell showed a decrease in the concentration of calcium when $Se^{(IV)}$ solutions are injected into the fluid cell compared to the concentration measured in selenium-free solution (Figure S2).

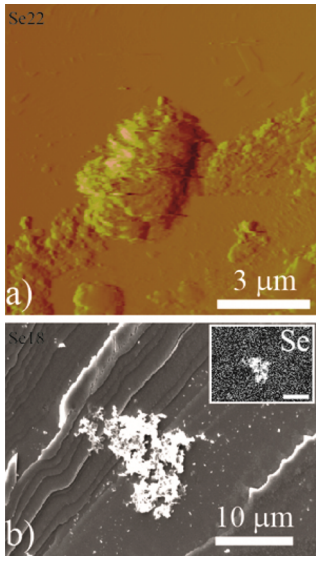

Figure 3. (a) AFM image of a selenium-rich phase that has precipitated from a 70 ppm selenite solution. The precipitate is 3 μm wide and 350 nm thick. (b) SEM image of a selenium-rich phase that has precipitated in an area with several steps on a calcite surface. The inset displays an EDX element map of selenium in the same image, demonstrating that selenium was incorporated into the precipitate.

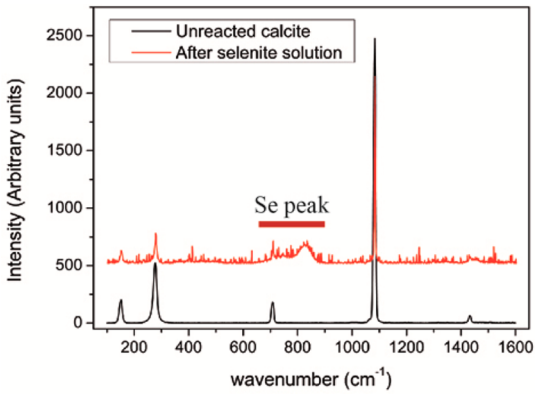

Figure 4. Raman spectra of the calcite crystal used for the experiments and the selenium precipitates (see Figure 3b). The peaks corresponding to the selenite stretching modes are also indicated and are located in the range of other selenium phases (see the Supporting Information).

As well, it was found that the concentration of selenium decreases with time during the dissolution experiments performed using these solutions. This indicates that both Ca^{2+} and $Se^{(IV)}$ were retained in the cell, possibly forming a Ca selenite phase. This phase is most likely $CaSeO_3{\cdot}H_2O$, which is the most stable calcium selenite phase within the range of pH 3 to 12.[22,30] Conversely, the concentration of selenium in the outflow of the AFM experiments performed using $Se^{(VI)}$ solutions mostly remained constant (within the limits of measurement error), indicating no removal of $Se^{(VI)}$, in agreement with AFM observations showing limited precipitation in these experiments (Figure S2). Also, calcium concentration in the outflow of these experiments remained approximately constant or even showed an increase compared to the values measured in pure water, which is an indication that in this case, no detectable calcium precipitation takes place.

Epitaxial Relationships between Ca-Selenite and Calcite. The larger flatter particles formed on the calcite surface in the presence of $Se^{(IV)}$ appear oriented on the substrate and tend to elongate following specific directions (Figure 5), possibly implying some degree of crystallographic control on the nucleation and growth of the calcium selenite phase by the underlying calcite surface (i.e., epitaxy).

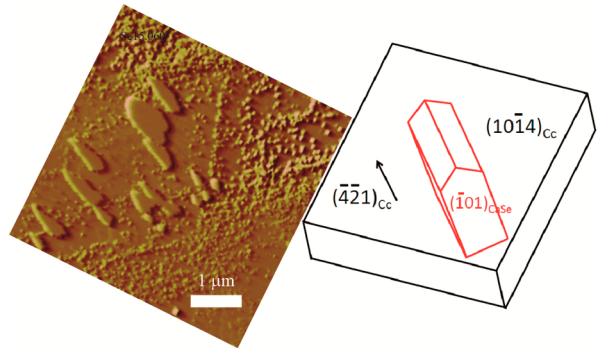

Figure 5. Left: AFM image showing the epitaxial growth of the selenium precipitate. Right: Potential epitaxial relationship between a calcite cleavage surface and $CaSeO_3{\cdot}H_2O$ simulated using the SHAPE software.

In particular, Ca-selenite precipitates seem to orientate and elongate parallel to the short diagonal of the rhombohedral dissolution etch pits formed on calcite, i.e. the [-4−21] direction. Possible epitaxial relationships were studied considering that $CaSeO_3{\cdot}H_2O$ is the likely phase formed during AFM experiments. Calcium selenite monohydrate crystallizes in the monoclinic system, space group $P2_1/c$. The unit cell parameters are a = 7.622, b = 6.745, c = 7.922 Å and β = 108.46°. A sketch of the $CaSeO_3{\cdot}H_2O$ structure and its calculated morphology is shown in Figure 5. A good structural matching was found between the [−4−21] direction in calcite and the $[001]_{CaSe}$ direction. The Ca−Ca distance along the [−4−21] direction in calcite is 4.084 Å. In the $CaSeO_3{\cdot}H_2O$ structure, zigzag calcium chains run approximately parallel to the [001] direction, with a Ca−Ca distance of 4.234 Å.

Additionally, the Ca−Ca distance along the [010] direction in $CaSeO_3{\cdot}H_2O$ was found to be 6.745 Å, which approximates well the Ca−Ca distance along the [−441] direction in calcite (6.425 Å). However, simultaneous matching along both sets of directions is highly unlikely, as the angular misfit is significant (51° vs 69°). This could explain why continuous Ca selenite epitaxial layers are not observed on calcite surfaces but thick 3D-crystals that elongated preferentially parallel to the −-421] direction of calcite are. Nevertheless, a likely epitaxial relationship was simulated using the SHAPE software (http://www.shapesoftware.com/) considering the following epitaxial relationship between calcite (Cc) and $CaSeO_3{\cdot}H_2O$ (CaSe): $(10{-}14)_{Cc}\|(100)_{CaSe}$ and $[{-}4{-}21]_{Cc}\|[001]_{CaSe}$ (Figure 5). Note that the $(100)_{CaSe}$ plane contains both the [010] and [001] directions, and the $(10{-}14)_{Cc}$ plane contains both the [−4−21] and [−441] directions.

Height values of calcium selenite islands measured in AFM experiments range from a minimum of ca. 1.5 nm up to 14.5 nm after around 1 h of reaction. The values most frequently found were ca. 3.7, 4.4, 5.7, and 6.2 nm (Figure 5). Interestingly, these heights are approximately integer multiples of the thickness of half a $CaSeO_3{\cdot}H_2O$ monolayer (in the

direction perpendicular to the (100) plane), which would be in agreement with the proposed epitaxial relationship. Nevertheless, this needs further confirmation by diffraction (2D-XRD) or spectroscopic (e.g., μ-XRD, μ-XAS, and/or μ-FTIR) techniques, a topic of possible future investigations.

The existence of a structural matching between calcite and $CaSeO_3 \cdot H_2O$ is an important factor to consider when studying the selenium sequestering capability of calcite, particularly in flow-through systems. From an energetic point of view, heterogeneous nucleation (on the calcite substrate) is a more favorable process than homogeneous nucleation in the bulk solution. Furthermore, $CaSeO_3 \cdot H_2O$ precipitation at low supersaturation will be facilitated by epitaxial nucleation as a result of the good matching between $CaSeO_3 \cdot H_2O$ and calcite structures. This will in turn enhance the removal of $Se^{(IV)}$ from aqueous solutions.

Dissolution–Crystallization Pathway for Selenium Removal from Aqueous Solutions: Thermodynamic Drive and the Role of the Fluid Boundary Layer. Initially, all solutions used in dissolution experiments were undersaturated with respect to any possible precipitating phase. The absence of Ca^{2+} and CO_3^{2-} in the injecting fluid ensured far-from-equilibrium conditions with respect to the calcite surface, so that it will immediately dissolve once in contact with Se-bearing solutions. The adsorption process was simulated with PHREEQC using two approaches: exchange with the selenite solutions (a) before contact with calcite (i.e., as if all adsorption would take place before calcite starts dissolving, no carbonate or bicarbonate ions in solution) and (b) after equilibration with calcite (i.e., as if calcite dissolution is fast compared to adsorption). As our experiments were performed under constant flow, equilibrium with respect to calcite would not be reached. Thus, the real situation will be constrained by these two extreme cases. These simulations are used exclusively to determine the amount of selenite adsorbed onto calcite. Subsequently, the initial solution composition was modified by subtracting the amount of selenium adsorbed from the initial amount in the solution. However, both simulations gave the same results. In our case, the small surface area of the calcite fragment (considered here as the geometric surface area of a typical crystal used in the AFM experiments exposed to the solution, 26 mm^2) results in a small number of effective sites for exchange and thus in limited selenite adsorption compared to the initial number of moles of selenium present in solution (Table S1). Nevertheless, if the adsorption takes place on a substrate of higher surface area, this process may be more important.

PHREEQC simulations of the interaction between calcite and Se-bearing solutions (under conditions similar to those of our AFM experiments) indicate that if calcite dissolves until equilibrium in a 70 ppm $Se^{(IV)}$ solution is reached, the resulting solution is undersaturated with respect to any possible phase, including the most stable Ca-selenite phase ($CaSeO_3 \cdot H_2O$). The same applies for a 200 ppm $Se^{(IV)}$ solution, as well as the 70 and 200 ppm $Se^{(VI)}$ solutions. Saturation states with respect to the relevant phases found in these simulations are given in the Supporting Information (Table S3). The scenario considered above assumes that all of the dissolved calcite will mix with the entire solution and a solid in equilibrium with this solution will precipitate. This is however, an oversimplification. In most of the cases, dissolution and precipitation processes are confined to a fluid boundary layer at the reaction interface with a different composition from the bulk. The existence of such an interfacial fluid layer, defined by steep cation concentration gradients close to the surface of the mineral, was observed by Putnis et al.[31] during mineral replacement reactions using real-time phase-shift interferometry. Thus, we performed a second set of simulations considering that the reaction process takes place in a series of small reaction steps (see Supporting Information, Table S4). In each of these steps, a calcite monolayer (i.e., 0.3 nm thick) from a $4 \times 3 \times 1$ mm crystal (2.1×10^{-10} moles) dissolves in a thin layer of solution of defined thickness (from 1 nm to 1 mm). Although this scenario is still a simplification, as it is considered that the composition within the thin layer of fluid is homogeneous, it is a closer approach to reality. The saturation state of this fluid layer of the different experimental solutions with respect to possible precipitating selenium-bearing phases was calculated assuming that no precipitation takes place (Table S4). It was found that for thicknesses smaller than 10 μm, this fluid layer in the $Se^{(IV)}$ solutions is supersaturated with respect to $CaSeO_3 \cdot H_2O$. However, it remains undersaturated with respect to any possible phase in the case of $Se^{(VI)}$ solutions, regardless of the thickness of the boundary layer considered or the selenium concentration. This is consistent with the idea that, generally, the more oxidized selenium species are more soluble.[8]

PHREEQC calculations are fully in agreement with our AFM observations and provide indirect evidence of the existence of a fluid boundary layer in close contact with the mineral surface whose composition will ultimately determine the progress of coupled dissolution–precipitation reactions. Furthermore, in this case, the fact that the nucleation of the Ca-selenite phase occurs preferentially in areas of high step density is consistent with a local faster release of Ca to the solution in contact with the surface in these areas, and not enough time to equilibrate by diffusion to the bulk solution before the buildup of enough supersaturation with respect to the secondary phase, that then precipitates. The chosen flow rate ensured that diffusion within the bulk solution was minimal. Thus, it seems clear that the interaction of $Se^{(IV)}$ solutions with calcite is an interface-coupled dissolution–precipitation process.[32,33] Similar coupled processes have been recently described, for example, by Daval et al.[34] during the carbonation of wollastonite, Hövelmann et al.[35] from direct observations of the precipitation of a hydrated $MgCO_3$ phase during the carbonation of brucite, Ruiz-Agudo et al.[36] during the dissolution of wollastonite, and Urosevic et al.[37] during the coupled dissolution of dolomite and the precipitation of another Mg-carbonate phase. In these previous described examples, the bulk solution flowing out of the reaction cell was, as in the present case, undersaturated with respect to any phase, but nevertheless a precipitate was observed forming on the surface.

Implications and Environmental Relevance. AFM is used in this study as the optimal technique for elucidating the mechanisms of fluid–mineral interactions by directly observing processes in action (e.g., see the review by Ruiz-Agudo and Putnis,[11] and references therein). Upon contact with $Se^{(IV)}$ bearing solutions, calcite dissolves by nucleation and spreading of etch pits, while, simultaneously, a precipitate (most likely calcium selenite, $CaSeO_3 \cdot H_2O$) nucleates and grows on the surface. However, calcite dissolution in the presence of $Se^{(VI)}$ does not result in any significant precipitation. Thus, our results suggest that $Se^{(IV)}$ is selectively retained in a new phase on calcite surfaces (as opposed to $Se^{(VI)}$) during calcite dissolution. Interestingly, Renard et al.[16] have also found that during calcite growth, selenite ($Se^{(IV)}$) is incorporated into growth hillocks,

whereas selenate ($Se^{(VI)}$) is not. In this case, the explanation for this selective behavior is given by the differences in the $Se^{(IV)}$ and $Se^{(VI)}$ coordination, as both oxyanions have a similar charge (2-). The selenate anion SeO_4^{2-} has a tetrahedral shape, while the selenite SeO_3^{2-} anion assumes a pyramidal-trigonal coordination in solution and thus would be easier to incorporate into a growing calcite step edge by substituting the planar trigonal carbonate group. However, during calcite dissolution a likely scenario for selenium removal must consider selenite adsorption and, more importantly, the formation of a calcium selenite precipitate, despite the fact that the bulk solution is undersaturated with respect to any selenite or selenate phase. Initially, calcite dissolves by the formation and spreading of rhombohedral etch pits, releasing Ca^{2+} and CO_3^{2-} to the solution. The solution in contact with the mineral locally becomes supersaturated with respect to the Ca selenite phase ($CaSeO_3{\cdot}H_2O$), which then precipitates. The growth of this calcium selenite phase is facilitated by the good epitaxial matching between this phase and calcite. Its precipitation decreases the calcium concentration of the fluid in contact with the mineral surface, and calcite continues to dissolve—as seen in the spreading of the rhombohedral etch pits.

Our study shows that calcite could be used successfully for selectively removing $Se^{(IV)}$ from aqueous solutions by a dissolution−precipitation process. Therefore, calcium carbonate could be employed as an effective barrier to clean polluted waters containing excess Se, such as acid mine drainage. These dissolution−precipitation processes would continue while enough Se is present or if the flow is continuous, and if the solution is in contact with the fresh, unreacted calcite substrate. It was observed that during the experiments the calcite surfaces became increasingly covered by the precipitating Se phase. This could lead eventually to passivation of the calcite surface in time. However, if porosity or other fluid pathways are generated during the reaction the selenium bearing solution will be continuously in contact with the unreacted calcite. Nevertheless, a substrate of high surface area, such as finely crushed limestone, could be more effective as it would provide more nucleation and precipitation sites.

Finally, these results also imply that calcite—a ubiquitous mineral at the Earth's surface, in the form of limestones—may have already played a significant role as a sink of $Se^{(IV)}$ from ocean waters given its ability to trap $Se^{(IV)}$ oxyanions under both close-to-equilibrium and highly undersaturated conditions (through a dissolution−precipitation process), providing an explanation for the higher $Se^{(VI)}$ signature of the ocean chemistry.[15]

■ ASSOCIATED CONTENT

Ⓢ Supporting Information

Reference Raman spectra of selenium minerals are provided. The chemical analysis of fluid composition and thermodynamic calculations are given. This material is available free of charge via the Internet at http://pubs.acs.org.

■ AUTHOR INFORMATION

Corresponding Author

*E-mail: francois.renard@ujf-grenoble.fr.

Notes

The authors declare no competing financial interest.

■ ACKNOWLEDGMENTS

We are grateful to the Institut Universitaire de France and the CNRS, for providing financial support for this work. The authors thank V. Rapelius for help with ICP-OES analyses. The experimental facilities in the Institut für Mineralogie, University of Münster, are supported by the German Research Council (DFG). E.R.-A. also acknowledges the receipt of a Ramón y Cajal grant from Spanish Ministry of Economy and Competitiveness, as well as additional funding from the Spanish Government (grant MAT2012-37584) and the Junta de Andalucía (research group RNM-179 and project P11-RNM-7550).

■ REFERENCES

(1) Paquette, J.; Reeder, R. J. Relationship between surface structure, growth mechanism, and trace element incorporation in calcite. *Geochim. Cosmochim. Acta* **1995**, *59*, 735−749.

(2) Rimstidt, J. D.; Balog, A.; Webb, J. Distribution of trace elements between carbonate minerals and aqueous solutions. *Geochim. Cosmochim. Acta* **1998**, 1851−1863.

(3) Davis, K. J.; Dove, P. M.; De Yoreo, J. J. The role of Mg^{2+} as an impurity in calcite growth. *Science* **2000**, *290*, 1134−1137.

(4) Stipp, S. L. S.; Christensen, J. T.; Lakshtanov, L. Z.; Baker, J. A.; Waight, T. Rare Earth element (REE) incorporation in natural calcite: upper limits for actinide uptake in a secondary phase. *Radiochim. Acta* **2006**, *94*, 523−528.

(5) Dove, P. M.; Hochella, M. F., Jr. Calcite precipitation mechanisms and inhibition by orthophosphate: in situ observations by scanning force microscopy. *Geochim. Cosmochim. Acta* **1993**, *57*, 705−714.

(6) Alexandratos, V. G.; Elzinga, E. J.; Reeder, R. J. Arsenate uptake by calcite: macroscopic and spectroscopic characterization of adsorption and incorporation mechanisms. *Geochim. Cosmochim. Acta* **2007**, *71*, 4172−4187.

(7) Montes-Hernandez, G.; Concha-Lozano, N.; Renard, F.; Quirico, E. Removal of oxyanions from synthetic wastewater via carbonation process of calcium hydroxide: fundamentals and applications. *J. Hazard. Mater.* **2009**, *166*, 788−795.

(8) Aurelio, G.; Fernandez-Martinez, A.; Cuello, G. J.; Roman-Ross, G.; Alliot, I.; Charlet, L. Structural study of selenium(IV) substitutions in calcite. *Chem. Geol.* **2010**, *270*, 249−256.

(9) Montes-Hernandez, G.; Sarret, G.; Hellmann, R.; Menguy, N.; Testemale, D.; Charlet, L.; Renard, F. Nanostructured calcite precipitated under hydrothermal conditions in the presence of organic and inorganic selenium. *Chem. Geol.* **2011**, *290*, 109−120.

(10) Morse, J. W.; Ardvison, R. S. The dissolution kinetics of major sedimentary carbonate minerals. *Earth-Sci. Rev.* **2002**, *58*, 51−84.

(11) Ruiz-Agudo, E.; Putnis, C. V. Direct observations of mineral-fluid reactions using Atomic Force Microscopy: the specific example of calcite. *Mineral. Mag.* **2012**, *76*, 227−253.

(12) Winkel, L. E. H; Johnson, A.; Lenz, M.; Grundl, T.; Leupin, O. X.; Amini, M.; Charlet, L. Environmental selenium research: From microscopic processes to global understanding. *Environ. Sci. Technol.* **2011**, *46*, 571−579.

(13) Levander, O. A.; Burk, R. F. Update of human dietary standards for selenium. In *Selenium: Its Molecular Biology and Role in Human Health*, 2nd ed.; Hatfield, D. L., Berry, M. J., Gladyshev, V. N., Eds.; Springer: New York, 2006.

(14) *Opinion of the Scientific Committee on Food on the Revision of Reference Values for Nutrition Labelling*; European Commission Scientific Committee on Food: Brussels, 2003.

(15) Conde, J. E.; Sanz Alaejos, M. Selenium concentrations in natural and environmental waters. *Chem. Rev.* **1997**, *97*, 1979−2003.

(16) Renard, F.; Montes-Hernandez, G.; Ruiz-Agudo, E.; Putnis, C. V. Selenium incorporation into calcite and its effect on crystal growth: An atomic force microscopy study. *Chem. Geol.* **2013**, *340*, 151−161.

(17) Montes-Hernandez, G.; Renard, F.; Lafay, R. Experimental assessment of CO_2-mineral-toxic ion interactions in a simplified freshwater aquifer: Implications for CO_2 leakage from deep geological storage. *Environ. Sci. Technol.* **2013**, *47*, 6247−6253.
(18) Little, M. G.; Jackson, R. B. Potential impacts of leakage from deep CO_2 geosequestration on overlying freshwater aquifers. *Environ. Sci. Technol.* **2010**, *44*, 9225−9232.
(19) Putnis, C. V.; Ruiz-Agudo, E. The mineral-water interface: Where minerals react with the environment. *Elements* **2013**, *9* (3), 177−182.
(20) Parkhurst, D. L.; Appelo, C. A. J. *Users Guide to PHREEQC (version 2) A Computer Program for Speciation, Batch Reaction, One Dimensional Transport and Inverse Geochemical Calculations*; Water-Resources Investigation report 99-4259, U.S. Geological Survey: Washington, DC, 1999; p 312.
(21) Wojdyr, M. Fityk: A general-purpose peak fitting program. *J. Appl. Crystallogr.* **2010**, *43*, 1126−1128.
(22) Cornelis, G.; Poppe, S.; van Gerven, T.; van der Broeck, E.; Ceulemans, M.; Vandecasteele, C. Geochemical modelling of arsenic and selenium leaching in alkaline water treatment sludge from the production of non-ferrous metals. *J. Hazard. Mater.* **2008**, *159*, 271−279.
(23) Cowan, C. E.; Zachara, J. M.; Resch, C. T. Solution ion effects on the surface exchange of selenite on calcite. *Geochim. Cosmochim. Acta* **1990**, *54*, 2223−2234.
(24) Ruiz-Agudo, E.; Kowacz, M.; Putnis, C. V.; Putnis, A. The role of background electrolytes on the kinetics and mechanism of calcite dissolution. *Geochim. Cosmochim. Acta* **2010**, *74*, 1256−1267.
(25) Cheng, L.; Lyman, P. F.; Sturchio, N. C.; Bedzyk, M. J. X-ray standing wave investigation of the surface structure of selenite anions adsorbed on calcite. *Surf. Sci.* **1997**, *382* (1), L690−L695.
(26) Piana, S.; Jones, F.; Gale, J. D. Assisted desolvation as a key kinetic step for crystal growth. *J. Am. Chem. Soc.* **2006**, *128*, 13568−13574.
(27) Stack, A. G.; Raiteri, P.; Gale, J. D. Accurate rates of the complex mechanisms for growth and dissolution of minerals using a combination of rare event theories. *J. Am. Chem. Soc.* **2012**, *134*, 11−14.
(28) Arvidson, R. S.; Collier, M.; Davis, K. J.; Vinson, M. D.; Amonette, J. E.; Luttge, A. Magnesium inhibition of calcite dissolution kinetics. *Geochim. Cosmochim. Acta* **2006**, *70*, 583−594.
(29) Lea, A. S.; Amonette, J. E.; Baer, D. R.; Liang, Y.; Colton, N. G. Microscopic effects of carbonate, manganese and strontium ions on calcite dissolution. *Geochim. Cosmochim. Acta* **2001**, *65*, 369−379.
(30) Nishimura, T.; Hata, R.; Hasegawa, F. Chemistry of the M (M = Fe, Ca, Ba)-Se-H_2O systems at 25 °C. *Molecules* **2009**, *14*, 3567−3588.
(31) Putnis, C. V.; Tsukamoto, K.; Nishimura, Y. Direct observations of pseudomorphism: compositional and textural evolution at a fluid-solid interface. *Am. Mineral.* **2005**, *90*, 1909−1912.
(32) Putnis, A. Mineral replacement reactions: from macroscopic observations to microscopic mechanisms. *Mineral. Mag.* **2002**, *66*, 689−708.
(33) Putnis, A.; Putnis, C. V. The mechanism of reequilibration of solids in the presence of a fluid phase. *J. Solid State Chem.* **2007**, *180*, 1783−1786.
(34) Daval, D.; Martinez, I.; Guigner, J.-M.; Hellmann, R.; Corvisier, J.; Findling, N.; Dominici, C.; Goffé, B.; Guyot, F. Mechanism of wollastonite carbonation deduced from micro- to nanometer length scale observations. *Am. Mineral.* **2009**, *94*, 1707−1726.
(35) Hövelmann, J.; Putnis, C. V.; Ruiz-Agudo, E.; Austrheim, H. Direct nanoscale observations of CO_2 sequestration during brucite [$Mg(OH)_2$] dissolution. *Environ. Sci. Technol.* **2012**, *46*, 5253−5260.
(36) Ruiz-Agudo, E.; Putnis, C. V.; Rodriguez-Navarro, C.; Putnis, A. The mechanism of leached layer formation during chemical weathering of silicate minerals. *Geology* **2012**, *40*, 947−950.
(37) Urosevic, M.; Rodriguez-Navarro, C.; Putnis, C. V.; Cardell, C.; Putnis, A.; Ruiz-Agudo, E. *In situ* nanoscale observations of the dissolution of (10−14) dolomite cleavage surfaces. *Geochim. Cosmochim. Acta* **2012**, *80*, 1−13.